

Microphysics and chemistry of sulphate aerosols at warm stratospheric temperatures

K. Drdla, R. F. Pueschel, and A. W. Strawa

Atmospheric Physics Branch, NASA Ames Research Center, Moffett Field, California

R. C. Cohen

Department of Chemistry, University of California, Berkeley

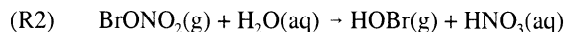
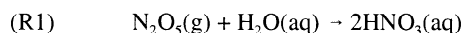
T. F. Hanisco

Department of Chemistry, Harvard University, Cambridge, Massachusetts

Abstract. Observations of high NO_x/NO_y ratios (overall 40% larger than modelled values) during the Polar Ozone Loss in the Arctic Region in Summer campaign have led us to re-examine the heterogeneous chemistry of stratospheric aerosol particles during the polar summer period, using the Integrated MicroPhysics and Aerosol Chemistry on Trajectories model. The warm summer temperatures (up to 235 K) imply very concentrated sulphuric acid solutions (80 wt %). On the one hand, these solutions are more likely to freeze, into sulphuric acid monohydrate (SAM), reducing the efficiency of the N_2O_5 hydrolysis reaction. Including this freezing process increases NO_x/NO_y ratios but does not improve model/measurement agreement: in polar spring, SAM formation causes the NO_x/NO_y ratio to be overpredicted whereas freezing has a much smaller effect on nitrogen chemistry during the continuous solar exposure of polar summer. On the other hand, if sulphate aerosols remain liquid, the high acidity may promote acid-catalysed reactions. The most important reaction is $\text{CH}_2\text{O} + \text{HNO}_3$, which effectively increases NO_x/NO_y ratios across a wide range of conditions, improving agreement with measurements. Furthermore, the production of HONO can either enhance gas-phase OH concentrations or promote secondary liquid reactions, including $\text{HONO} + \text{HNO}_3$ and $\text{HONO} + \text{HCl}$. Primary uncertainties include the uptake coefficient of CH_2O relevant to reaction with HNO_3 , the amount of HONO available for secondary reaction, and the relative rates of HONO reaction with HNO_3 and HCl . The fate of the formic acid product, whose presence in the stratosphere may be an indicator for the CH_2O reaction, and the impact on the stratospheric hydrogen budget are also discussed.

1. Introduction

The majority of stratospheric aerosol particles are composed of aqueous sulphuric acid solutions [Turco *et al.*, 1982, and references therein]. Two heterogeneous reactions have been shown to be effective on sulphate aerosols throughout the stratosphere:

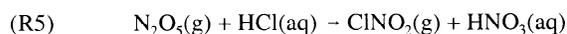
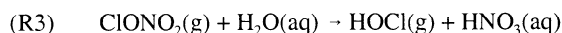


Reaction (R1), in particular, has been shown to have a widespread impact on stratospheric nitrogen (NO_y) partitioning, increasing the reservoir species, HNO_3 , at the expense of active nitrogen such as NO and NO_2 (NO_x) [McElroy *et al.*, 1992; Fahey *et al.*, 1993; Wilson *et al.*, 1993]. Reaction (R2) leads to HOBr formation, especially at night, causing a morning release of OH radicals [Hanson and Ravishankara, 1995; Lary *et al.*, 1996].

While these reactions are now commonly included in stratospheric chemistry models, it is not yet clear that our understanding of stratospheric nitrogen chemistry is complete. In

particular, observations made during the Polar Ozone Loss in the Arctic Region In Summer (POLARIS) campaign consistently found NO_x/NO_y ratios greater than could be explained by existing models [Gao *et al.*, 1999; Osterman *et al.*, 1999; K.K. Perkins *et al.*, manuscript in preparation, 1999]. Since sulphate aerosols have already been shown to affect the NO_x/NO_y ratio, via reaction (R1), this paper will examine recent theories on sulphate behaviour which may further affect modelled nitrogen partitioning.

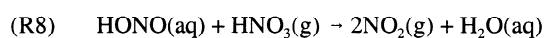
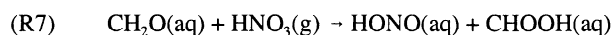
Several other reactions are known to occur on sulphate aerosols but have been shown to have little effect at temperatures above 200 K, for example:



However, these reactions share one characteristic: they are all promoted by the availability of water, either because H_2O is a reactant or because HCl is a reactant, and HCl requires H_2O to dissolve in solution [Hanson *et al.*, 1994; Hanson and Ravishankara, 1994]. All were initially investigated because of their effectiveness at cold temperatures, where condensed water is readily available.

For typical conditions at midlatitudes, however, the sulphate solutions are more concentrated in H₂SO₄ than for cold polar regions [Steele and Hamill, 1981]; consequently, water is less available for reaction, reducing the efficiency of reactions such as (R3)-(R6). Reactions (R1) and (R2) are exceptions that are able to remain equally effective across a wide range of sulphuric acid compositions. Mechanistic explanations for these reactions [Robinson *et al.*, 1997] have invoked a second reaction mechanism, promoted by increasing solution acidity, that balances the water-catalysed mechanism.

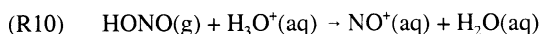
Other acid-catalysed reactions also exist, which can become more effective as solutions become more concentrated. Reactions with stratospheric potential include [Horváth *et al.*, 1988; Fenter and Rossi, 1996; Zhang *et al.*, 1996; Iraci and Tolbert, 1997; Longfellow *et al.*, 1998]:



In each case, the reactions are promoted by reactants (HONO and CH₂O) that become more soluble in acidic solutions [Becker *et al.*, 1996; Longfellow *et al.*, 1998; Tolbert *et al.*, 1993; Iraci and Tolbert, 1997]. These reactions have not previously been investigated in any stratospheric chemistry models.

Increased sulphate solution acidity can also promote substantial compositional changes in stratospheric aerosols, in particular, possible phase changes. Such a phase change can dramatically alter the efficiencies of all heterogeneous reactions, and therefore also needs to be considered to fully evaluate the chemical impact of sulphate aerosols.

The first such process to be proposed was the formation of nitrosyl sulphuric acid (NSA or NOHSO₄) [Burley and Johnston, 1992]. Laboratory studies have confirmed that HONO dissolves in acid solutions through formation of the nitrosyl ion (NO⁺) [Becker *et al.*, 1996; Zhang *et al.*, 1996]:



If nitrosyl builds up in solution, it can reach its solubility limit and precipitate out as solid NSA [Burley and Johnston, 1992]:



This compound has been tentatively identified in stratospheric aerosols [Farlow *et al.*, 1977]. Studies have shown that reaction of HCl, producing ClNO, is very efficient on NSA [Fenter and Rossi, 1996]; other reactions have not been studied. But Saastad *et al.* [1993] showed that the heterogeneous HONO formation mechanisms proposed by Burley and Johnston [1992], involving NO and NO₂, were not efficient. Also, laboratory studies have shown that HONO, while soluble, will not be present in stratospheric aerosols at the concentrations necessary for NSA precipitation [Becker *et al.*, 1996; Longfellow *et al.*, 1998]. Therefore, NSA formation has generally been discounted.

Another possibility is that warm temperatures can, seemingly paradoxically, cause stratospheric sulphate aerosols to freeze [Zhang *et al.*, 1995]. As the acidity increases, the solutions approach the composition of sulphuric acid monohydrate (SAM). Measurements show that the formation of this solid compound is thermodynamically favoured, and it forms in the laboratory more readily than other sulphuric acid hydrates [Zhang *et al.*, 1995]. Reaction (R3) and especially reaction (R1) have been measured to be less efficient on SAM than on liquid solutions [Zhang *et al.*, 1995].

This paper will investigate the likelihood of SAM and NSA formation and examine the impact of reactions (R7)-(R9) on the composition of the lower stratosphere. These processes are all promoted by the same conditions, namely the increased aerosol acidity which occurs at warm stratospheric temperatures. The POLARIS campaign primarily sampled polar stratospheric summer conditions, when elevated temperatures occur. Furthermore, the observed NO_x/NO_y ratios, consistently 40% higher than model predictions, demonstrate that current models do not properly account for stratospheric nitrogen chemistry. The wealth of measurements available on NASA's ER-2 aircraft allows for thorough evaluation of these various processes, to examine which may be occurring and how they may interact.

In addition, a survey of previous ER-2 campaigns revealed that the ER-2 had also sampled similar temperature conditions in the Antarctic, at the end of the Airborne Southern Hemisphere Ozone Experiment and Measurements for Assessing the Effects of Stratospheric Aircraft (ASHOE/MAESA) campaign. These data will be used to supplement the POLARIS data, providing insight on whether similar behaviour is seen in the Southern Hemisphere and extending the temperature and NO_x/NO_y regimes.

2. Measurements

The POLARIS campaign sampled the arctic polar region during the summer of 1997 through a series of ER-2 flights, using a wide range of instruments, as described in this special issue. Table 1 lists the measurements and data products that have been used in this study, either for model initialization or for comparison with model results. Table 2 provides a list of flight dates that have been used in the analysis, with a few key characteristics of the flights; the selection of data points will be described in more detail in section 3.

The POLARIS campaign focussed on ozone loss during summer in the northern polar regions and consequently tended to sample air

Table 1. ER-2 Measurements Used in this Study.

Measurement	Reference
<i>Measurements Used for Model Initialization</i>	
Sulphate aerosol surface area	Wilson <i>et al.</i> [1992]
H ₂ O	Hintsa <i>et al.</i> [1999] or May [1998] (for ASHOE/MAESA: Kelly <i>et al.</i> [1993])
NO _y	Gao <i>et al.</i> [1999]
O ₃	Proffitt <i>et al.</i> [1993]
Cl _y	Montzka <i>et al.</i> [1996]
Br _y	Wamsley <i>et al.</i> [1998]
Column ozone	McPeters <i>et al.</i> [1998] and McElroy [1995]
Surface reflectivity	McPeters <i>et al.</i> [1998] and McElroy [1995]
<i>Additional Measurements Used for Model Initialization*</i>	
N ₂ O	Loewenstein <i>et al.</i> [1990]
CH ₄	Webster <i>et al.</i> [1994]
<i>Measurements to Which Model Data are Compared</i>	
NO	Gao <i>et al.</i> [1999]
NO ₂	K.K. Perkins <i>et al.</i> , manuscript in preparation, 1999 (not available during ASHOE/MAESA) or Del Negro <i>et al.</i> [this issue]
OH	T.F. Hanisco <i>et al.</i> , manuscript in preparation, 1999
ClO	Stimpfle <i>et al.</i> [this issue]
ClONO ₂	Stimpfle <i>et al.</i> [this issue] (not available during ASHOE/MAESA)
HCl	Webster <i>et al.</i> [1994]

*Measurements in this list were used when available; however, simulations were still done in the absence of these data, using estimated values.

Table 2. Summary of Flights Being Simulated, Flight Conditions, and Model/Measurement (NO+NO₂)/NO_y Discrepancies for Key Model Scenarios

Date	Number of Modelled Points	Average flight conditions					Average (NO+NO ₂)/NO _y Discrepancy (Model/Measured)			
		Latitude	Solar Zenith Angle	Temperature, K	Aerosol H ₂ SO ₄ Content, wt %	S _{SAM} , K	Baseline	SAM (100% at S _{SAM} =0K)	Scenario C1: Reactions (R7), (R8), and (R9) (γ _{CH₂O} = 1)	Scenario C2: Reactions (R7), (R8), and (R9) (Tolbert γ _{CH₂O})
<i>ASHOE/MAESA Flights</i>										
941010	16	-57.6	57.2	229.4±1.9	77.7±1.1	32.7±5.2	0.91±0.12	1.31±0.21	1.23±0.16	1.03±0.12
941013	17	-56.5	56.5	230.5±1.6	78.1±0.7	34.3±3.2	0.93±0.09	1.44±0.12	1.25±0.15	1.06±0.10
941016	17	-56.9	54.7	233.7±4.9	79.1±1.9	34.7±6.6	0.98±0.08	1.46±0.14	1.32±0.20	1.10±0.13
941020	14	-56.6	49.7	226.7±2.3	76.4±1.6	27.1±10.0	0.99±0.10	1.18±0.16	1.32±0.24	1.08±0.15
Overall	64						0.95±0.09	1.36±0.16	1.28±0.18	1.07±0.12
<i>POLARIS Flights</i>										
970422	46	25.1	31.1	205.3±3.0	64.4±2.6	0.0±0.0	0.73±0.04	0.73±0.05	0.95±0.08	0.76±0.04
970424	35	51.2	45.1	219.7±4.8	73.6±2.7	15.4±12.9	0.70±0.07	0.80±0.10	0.92±0.11	0.76±0.06
970426	53	77.7	68.9	224.7±3.1	75.7±1.9	25.0±10.1	0.68±0.06	0.81±0.10	0.88±0.10	0.73±0.07
970430	41	64.2	92.2	228.0±1.2	76.9±0.8	29.9±5.3	0.73±0.05	0.97±0.12	1.01±0.08	0.82±0.05
970502	50	69.6	61.4	228.4±1.0	77.6±0.5	34.1±2.1	0.75±0.04	1.02±0.06	1.01±0.06	0.82±0.04
970506	44	72	59.4	230.9±1.8	78.2±0.8	34.8±3.2	0.72±0.05	0.96±0.04	1.01±0.08	0.81±0.04
970509	37	64.5	91	228.4±0.5	77.4±0.3	32.6±1.8	0.73±0.03	1.05±0.03	1.03±0.10	0.83±0.04
970513	19	74	59	230.1±1.7	77.7±1.0	32.1±5.3	0.75±0.06	0.96±0.07	1.04±0.14	0.84±0.07
970626	46	66	49.1	226.3±1.9	76.5±0.9	28.6±5.0	0.72±0.05	0.82±0.07	1.11±0.13	0.82±0.05
970629	20	57.7	36.8	224.8±1.1	75.8±0.7	25.8±5.0	0.72±0.09	0.85±0.10	1.07±0.14	0.82±0.08
970630	21	64.9	43.3	225.8±1.3	75.6±1.6	23.1±9.3	0.66±0.08	0.77±0.12	1.09±0.14	0.79±0.07
970704	57	59.3	42	224.2±2.8	75.4±2.4	24.1±8.9	0.73±0.07	0.85±0.10	1.05±0.11	0.82±0.05
970707	55	77.4	57.9	230.8±1.3	78.3±0.8	35.1±3.7	0.75±0.03	0.84±0.02	1.07±0.08	0.83±0.02
970710	3	65.3	43.2	228.3±0.7	76.2±0.4	25.0±2.3	0.71±0.05	0.98±0.05	1.25±0.23	0.90±0.11
970908	50	76.7	74.6	222.8±1.6	75.0±0.6	21.6±3.9	0.72±0.07	1.08±0.13	1.00±0.08	0.82±0.05
970911	27	64.5	87.4	222.4±0.8	74.9±0.2	20.8±1.9	0.61±0.04	1.04±0.07	0.88±0.12	0.71±0.06
970914	42	64.4	88	219.3±0.4	73.3±0.7	10.4±2.9	0.71±0.08	0.97±0.12	0.99±0.19	0.80±0.10
970915	45	64.6	87.6	220.0±0.4	73.7±0.6	13.3±3.2	0.74±0.05	0.99±0.11	1.02±0.13	0.83±0.04
970918	52	78.1	79	221.1±1.5	74.3±0.4	17.6±2.9	0.72±0.09	1.08±0.08	0.97±0.11	0.81±0.07
970919	46	64.5	67.8	224.0±1.0	75.6±0.3	24.7±1.6	0.78±0.04	1.12±0.11	1.02±0.03	0.85±0.03
970921	37	39	43.6	214.0±4.4	70.7±3.0	3.3±4.7	0.76±0.14	0.92±0.18	1.01±0.20	0.82±0.15
970923	33	6.8	29.4	207.5±2.6	67.0±3.2	0.0±0.0	0.72±0.03	0.72±0.03	0.97±0.05	0.76±0.04
Overall	859						0.72±0.06	0.93±0.09	1.00±0.11	0.80±0.06

Ranges represent data variability (one standard deviation). Dates are in YYYYMMDD format.

with temperatures higher than typical midlatitude conditions in the lower stratosphere. Figure 1 illustrates the range of measured temperatures, placing them in the context of the sulphuric acid phase diagram by using the simultaneous water vapour measurements to calculate the equilibrium sulphuric acid composition [Steele and Hamill, 1981]. Also shown is a curve representing how sulphate aerosols in an air parcel with a fixed water content representative of the ER-2 data (3×10⁻⁴ mb, or 5 ppm at 60 mb) would respond to temperature variations. The warm temperatures, up to 235 K, correspond to sulphuric acid equilibrium compositions of nearly 80 wt %. The data at weight percents below 70 were all collected at midlatitudes and the tropics (on the flights of 970422, 970424, 970921, and 970923).

A review of previous ER-2 campaigns found that similarly warm temperatures were also measured during the ASHOE/MAESA campaign [Gaines et al., 1995]. In particular, four flights south from Christchurch, New Zealand, in October of 1994 sampled temperatures above 225 K; on the 16th of October, stratospheric temperatures above 240 K were sampled. These points are also shown in Figure 1. These four flights complement the POLARIS data, by providing a view of the southern hemisphere and also by demonstrating polar spring a few weeks earlier than the POLARIS measurements. Generally similar instrumentation was available during ASHOE/MAESA; key differences are noted in Table 1.

A dominant feature of the POLARIS campaign was elevated NO_x/NO_y ratios; the measurements were on average 40% higher than model estimates using standard gas-phase chemistry [DeMore

et al., 1997], as shown in Figure 2. Measured (NO+NO₂)/NO_y, referred to here as the NO_x/NO_y ratio, is determined from separate measurements of NO, NO₂, and NO_y (see Table 1). As discussed elsewhere [Del Negro et al., this issue; K.K. Perkins et al., manuscript in preparation, 1999], the two NO₂ measurements differ by 6% on average; for simplicity, the two measurements have been averaged for this study. ASHOE/MAESA data is also included in Figure 2, demonstrating the lower NO_x/NO_y values and better model/measurement agreement observed during the earlier campaign.

Since the POLARIS campaign, several laboratories have reexamined the rates of two key gas-phase reactions. Under stratospheric conditions, it has been found that the reaction of OH with NO₂ is 10-30% slower than recommended by DeMore et al. [1997] [Brown et al., 1999a; Dransfield et al., 1999]; the reaction of OH with HNO₃ is 20-30% faster [Brown et al., 1999b]. Both these reaction rate changes have the effect of increasing the computed NO_x/NO_y ratio and substantially improving the agreement with the measured ratio [Gao et al., 1999; Osterman et al., 1999]. In our own sensitivity studies using these reaction rates, improvement with measured NO_x/NO_y ratios was also achieved, but the model was unable to account for the highest measured values (i.e., NO_x/NO_y > 0.15), falling 10% short on average. Similar results were reported by Gao et al. [1999] based on an analysis of the same ER-2 observations of NO_x/NO_y. Osterman et al. [1999] showed that a 35% decrease in the rate coefficient of the OH+NO₂ was required to best match MkIV balloon-borne measurements of

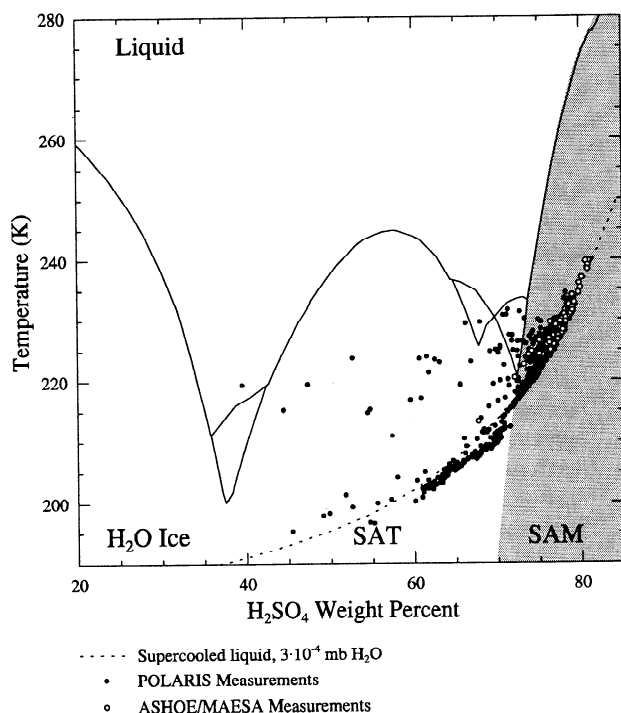


Figure 1. Sulphuric acid phase diagram [Gable *et al.*, 1950]. Curve shows evolution of a stratospheric air parcel with 3×10^{-4} mb of H₂O. Superimposed are the equilibrium sulphate compositions corresponding to the POLARIS (solid circles) and ASHOE/MAESA (open circles) data points modelled in this study. The SAM stability region is shaded gray.

NO_x/NO_y, which is larger than the 10-30% change in the rate suggested by the new laboratory data. However, use of both the Dransfield *et al.* [1999] rate for OH+NO₂ and the Brown *et al.* [1999b] rate for OH+HNO₃ leads to agreement (e.g., differences less than 10% at most altitudes) with the same MkIV measurements (G.Bo. Osterman and R.J. Salawitch, private communication, 1999). In summary, if these new laboratory rates for OH+NO₂ and OH+HNO₃ are valid, measured and modelled NO_x/NO_y ratios tend to agree within the combined uncertainties of the measurements and models, although a systematic discrepancy still seems to be present for the largest ER-2 observations of the NO_x/NO_y ratio. Better definition of the rates of these two key reactions is required before we can determine whether or not additional changes to stratospheric nitrogen chemistry are required.

3. The IMPACT Model

The Integrated MicroPhysics and Aerosol Chemistry on Trajectories (IMPACT) model was originally developed for simulations of polar stratospheric clouds, and therefore contains detailed treatments of aerosol microphysics and heterogeneous chemistry [Drdla, 1996]. Furthermore, the model's photochemistry and ability to simulate specific ER-2 data sets make it ideal for studies of aerosol effects on stratospheric chemistry.

The size distribution of sulphate aerosols is modelled using 51 size bins (~ 0.001 to $\sim 100 \mu\text{m}$ radius) which grow and shrink as the solution changes composition. Diffusion-limited dissolution of a wide range of species (HCl, HNO₃, HONO, CH₂O, and CHOOH) is calculated for each individual bin; separate components, for example NSA, can also be present within the same particle. NSA

precipitation will occur if its solubility limit [Burley and Johnston, 1992] is exceeded. Freezing and melting to/from SAM aerosols is explicitly calculated, with a second set of size bins for frozen aerosols.

Heterogeneous chemistry is calculated for each particle type and size bin. The baseline model includes reactions (R1)-(R6); reactions (R7)-(R9) and additional reactions discussed later are included in specific runs. To model these reactions, the solubility (according to the effective Henry's law coefficient, H^*) and diffusion is explicitly calculated. The fraction of the total diffusive flux available for reaction is specified by the reaction probability, γ ; the overall reaction rate is limited by the availability of both the reactants. Parameters used for these reactions are listed in Table 3; the combinations used in the various model scenarios are provided in Table 4.

The default reaction probability for reaction (R9) used here is 0.02, which is based on the laboratory measurements by Zhang *et al.* [1996] for a 71 wt % solution at 223 K. More recently, this reaction has also been studied by Longfellow *et al.* [1998], who measured details of the reaction kinetics, including solubilities and aqueous-phase reaction rates. In sensitivity tests (see Table 3), their parameterization of reaction (R9) has been implemented, with fixed values for the parameters H_{HCl} , D_b , and k^{II} (using the values measured for 70 wt % solutions at 215 K). Longfellow *et al.* [1998], however, found a much smaller reactivity ($\gamma \sim 2 \times 10^{-5}$) than Zhang *et al.* [1996]. Fenter and Rossi [1996] have also studied reaction (R9) but concluded that no reaction occurs for acidities greater than 65 wt %. This wide variability among the laboratory data has yet to be resolved. Furthermore, all the studies found the reactivity to be very sensitive to solution acidity and temperature, but no measurements of the reaction probability have been made at the high acidities relevant for POLARIS. (Note that even though the predicted HCl solubility in these concentrated solutions is low,

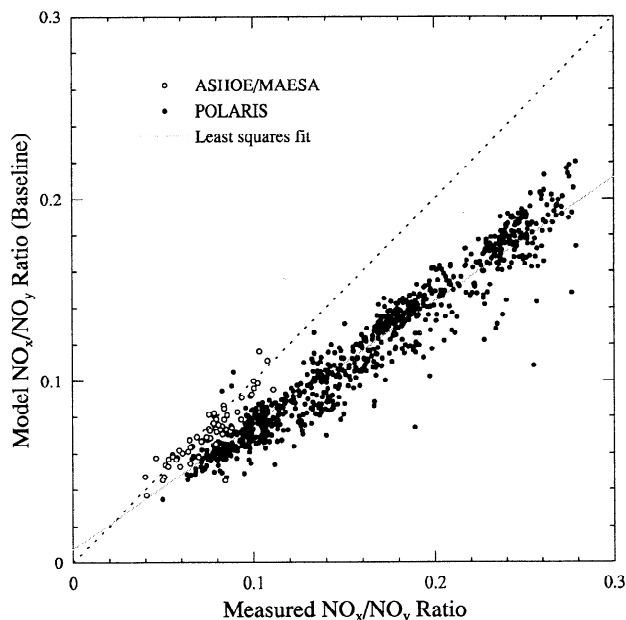


Figure 2. Cross plot of modelled and measured (NO+NO₂)/NO_y ratios, for the baseline model. See Table 1 for details of the measurements. POLARIS data is shown as solid circles; ASHOE/MAESA as open circles. All simulated points (see Table 2) are included. The line represents the least squares fit to the data.

Table 3. Parameters Used to Model Heterogeneous Reaction Rates

Parameter	Option	Value	Reference
(R1): $N_2O_3(g) + H_2O(aq) \rightarrow 2HNO_3(aq)$			
$\gamma_{N_2O_3}$	Liquid	0.1	<i>DeMore et al.</i> [1997]
	SAM	0.001	<i>Zhang et al.</i> [1995]
(R2): $BrONO_2(g) + H_2O(aq) \rightarrow HOBr(g) + HNO_3(aq)$			
γ_{BrONO_2}	Liquid	0.8	<i>DeMore et al.</i> [1997]
	SAM	0. or 0.8	
(R7): $CH_2O(aq) + HNO_3(g) \rightarrow HONO(aq) + ClHOI(aq)$			
$H^*_{CH_2O}$	Default	10^7 M/atm	<i>Iraci and Tolbert</i> [1997]
γ_{CH_2O}	Default	1	
	Tolbert	$\max(0.015, -0.529 + 8.13 \times 10^{-3} x_{H_2SO_4})$	<i>Tolbert et al.</i> [1993]
γ_{HNO_3}	Default	0.01	<i>Iraci and Tolbert</i> [1997]
(R8): $HONO(aq) + HNO_3(g) \rightarrow 2NO_2(g) + H_2O(aq)$			
H^*_{HONO}	Default	Fit to laboratory data	<i>Longfellow et al.</i> [1998]
	Becker	eqn (13) of <i>Becker et al.</i> [1996]	<i>Becker et al.</i> [1996]
γ_{HONO}	Default	1	
	Zhang	$-0.335 + 0.00537 x_{H_2SO_4}$	<i>Zhang et al.</i> [1996]
	Fenter	$\exp(-16.4 + 0.166 x_{H_2SO_4})$	<i>Fenter and Rossi</i> [1996]
γ_{HNO_3}	Default	0.01	<i>Iraci and Tolbert</i> [1997]
(R9): $HONO(aq) + HCl(g) \rightarrow ClNO(g) + H_2O(aq)$			
H^*_{HONO}	see entries for (R8)		
γ_{HONO}	see entries for (R8)		
γ_{HCl}	Default	0.02	<i>Zhang et al.</i> [1996]
	Longfellow	$\frac{4 H_{HCl} R T \sqrt{k^{\text{II}} [HONO]_{\text{aq}} D_l}}{\omega_{HCl}} f(r \sqrt{k^{\text{II}} [HONO]_{\text{aq}} / D_l})$	<i>Longfellow et al.</i> [1998]
(using values measured at 215 K, 70wt %)			
(R12): $CHOOH(aq) \rightarrow CO(g) + H_2O(aq)$			
H^*_{CHOOH}	Default	2.1×10^{-3} M/atm	<i>Iraci and Tolbert</i> [1997]
γ_{CHOOH}	Default	1	
k^I	Default	4.7×10^4 s ⁻¹	<i>Smith et al.</i> [1983]
(R13): $CHOOH(aq) + HNO_3(g) \rightarrow HONO(aq) + CO_2(g) + H_2O(aq)$			
H^*_{CHOOH}	Default	2.1×10^{-3} M/atm	<i>Iraci and Tolbert</i> [1997]
γ_{CHOOH}	Default	1	
γ_{HNO_3}	Default	0.0005	<i>Horváth et al.</i> [1988]
	Fast	0.01	

For γ_{HCl} , $x_{H_2SO_4}$ is H_2SO_4 weight percent and $[HONO]_{\text{aq}}$ is aqueous HONO concentration, M. Other parameters are as defined by *Longfellow et al.* [1998].

the laboratory data shows that reaction (R9) does occur on solutions with low HCl solubilities.) We have chosen to adopt the *Zhang et al.* [1996] value as a default, primarily because it does not require extrapolation of multiple parameters to high weight percents. Ultimately, more laboratory data, preferably providing the weight dependence of all the physical chemistry parameters, will be needed to resolve these questions; until then, any model treatment of this reaction is at best an approximation.

The model photochemical solver is based on *Elliott et al.* [1993], which uses a family approach with forward integration to provide stability with one-hour model time steps. For these studies, the model was configured with 57 species, grouped into 28 families, using 165 gas-phase reactions (of which 38 are photolysis reactions) with reaction rates based on *DeMore et al.* [1997]. Photolysis rates were calculated using the radiative transfer model

of *Salawitch et al.* [1994a] and *Prather* [1981]. Effects of Rayleigh scattering are considered, but aerosol scattering is ignored owing to the relatively low aerosol loading conditions that prevailed at the time of observation. The ozone column at each point along the back trajectory was determined from the Earth Probe Total Ozone Measuring Spectrometer (TOMS) measurements [*McPeters et al.*, 1998]. Ozone profiles were derived from these ozone columns by scaling climatological ozone profiles; the values were also scaled to match, at the final trajectory point, the Composition and Photodissociative Flux Measurements (CPFM) of the ozone column above the ER-2 [*McElroy*, 1995]. For the albedo, the TOMS reflectivity was used, and the pressure level of the reflecting surface was assumed to be 1013 mb; CPMF measurements of albedo and cloud height were used in place of the TOMS data for the final 12 hours of the trajectory.

Table 4. Liquid Reaction Model Scenarios

Scenario	H* _{HONO}	(R7): $\gamma_{\text{CH}_2\text{O}}$	(R8): γ_{HONO}	(R9): γ_{HCl}	Other Reactions
<i>HONO Uptake and Reactions (Section 5.1)</i>					
A1	Default	0	0	0	
A2	Becker	0	0	0	
A3	Default	0	0.01	0	
A4	Default	0	0	0.02	
<i>CH₂O Uptake and Reactions (Section 5.2)</i>					
B1	Default	1	0	0	
B2	Default	Tolbert	0	0	
B3	Default	1	0	0	(R12)
B4	Default	1	0	0	(R13), Default
B5	Default	1	0	0	(R13), Fast
<i>Combined Effects of Reactions (R7), (R8), and (R9) (Section 5.3)</i>					
C1	Default	1	0.01	0.02	
C2	Default	Tolbert	0.01	0.02	
C3	Default	1	0.01	0	
C4	Default	1	0	0.02	
C5	Default	Tolbert	0.01	0	
C6	Default	Tolbert	0.01	0	(R13), fast
C7	Default	Tolbert	0	0.02	
C8	Default	1	0	Longfellow	

See Table 3 for further details on parameters. Reactions (R1)-(R6) are included in all scenarios. Reactions (R12) and (R13) are not included unless specified in "Other reactions."

Simulations have been done for this study using backtrajectories provided by NASA Goddard [Schoeberl *et al.*, 1993]. For POLARIS flights, these trajectories are spaced about every 70 km along the flight track; for ASHOE/MAESA, they are spaced about every 320 km. All trajectories for which sufficient initialization data are available have been used in the analysis; Table 2 provides the numbers of trajectories used for each date. More than 90% of these points are above 100 mb; lower altitude points are found in aircraft descents, ascents, dives, and on stacked flights.

The model is initialized at the start of the trajectory using ER-2 measurements of long-lived tracers, as shown in Table 1, in a manner similar to previous investigations of ER-2 observations [i.e., Salawitch *et al.*, 1994a; Gao *et al.*, 1999]. The NO_x/NO_y ratio is initialized from the measured value at the end point. Since the model repartitions NO_y according to the chemistry over the ten-day trajectory, the final model NO_x/NO_y ratio is effectively independent of the initialization, allowing for meaningful comparisons between model and measurement values.

4. SAM Formation

Although stratospheric sulphate aerosols are generally observed to be liquid solutions, these liquid solutions are indeed supercooled (Figure 1) [Gable *et al.*, 1950; Turco *et al.*, 1982]. For typical stratospheric aerosols (40-70 wt %), the most stable phase for sulphate is sulphuric acid tetrahydrate (SAT). However, the extreme difficulty of nucleating SAT [i.e., Koop *et al.*, 1997] explains the presence of liquid solutions in preference to the thermodynamically stable solid phase.

Figure 1 also shows that the composition of the sulphate aerosol determines the solid phase into which a given solution will freeze. Composition, in turn, is a function of both the ambient water vapour pressure and the temperature, because the solution must maintain equilibrium with respect to the water vapour pressure. For example, temperature increases cause evaporation of water and therefore more acidic aerosols. At the temperatures experienced during POLARIS, Figure 1 shows that the most stable solid phase is sulphuric acid monohydrate (SAM), instead of SAT. (For

intermediate conditions, near 70 wt %, sulphuric acid dihydrate and trihydrate may also be stable, but their formation is not considered in this study.)

Laboratory studies [Zhang *et al.*, 1995] have found that SAM freezes more readily than SAT. Even at the warm temperatures necessary for acidic aerosols, substantial supercoolings of SAM (S_{SAM}) are possible; values of S_{SAM} up to 38 K were encountered in this analysis. Parameters such as freezing rates and critical solution activity products have not been determined for this system, which would be necessary to accurately predict when freezing will occur. Instead, this study will use a simple freezing parameterization, based on S_{SAM} , to evaluate several freezing scenarios and their impact on model chemistry.

Figure 3 demonstrates the evolution of temperature and H₂SO₄ weight percent for a single air parcel along a sample trajectory, corresponding to that sampled by the ER-2 at 75600 UT seconds on May 6, 1997 (970506). The initial temperature of 210 K is outside of the SAM stability regime, but as the temperature increases, the trajectory crosses into the SAM stability region and SAM becomes increasingly supercooled. (The SAM melting point can be determined in two distinct ways. The melting point of a fixed composition solution is the one relevant for calculating the SAM supercooling, i.e., the vertical difference in Figure 1. For SAM to be stable, the temperature must be less than this melting point. However, since stratospheric aerosols vary in composition as the temperature is altered, their composition will follow a curve such as that shown for 3×10⁻⁴ mb in Figure 1. Along this curve, the SAM stability region is exited at a very different point, identified here as the "SAM stability limit." Temperatures warmer than this stability limit indicate SAM stability.) The supercooling increases very rapidly initially, so that only an 8 K temperature increase is necessary to reach 30 K supercoolings.

Several possible scenarios for SAM formation are illustrated in Figure 3c. Uncertainties include the point at which freezing occurs, the proportion of particles that freeze, and the rapidity with which freezing occurs. The most widespread SAM formation is, of course, predicted if 100% of the particles instantaneously freeze when the melting point is crossed (0 K supercooling).

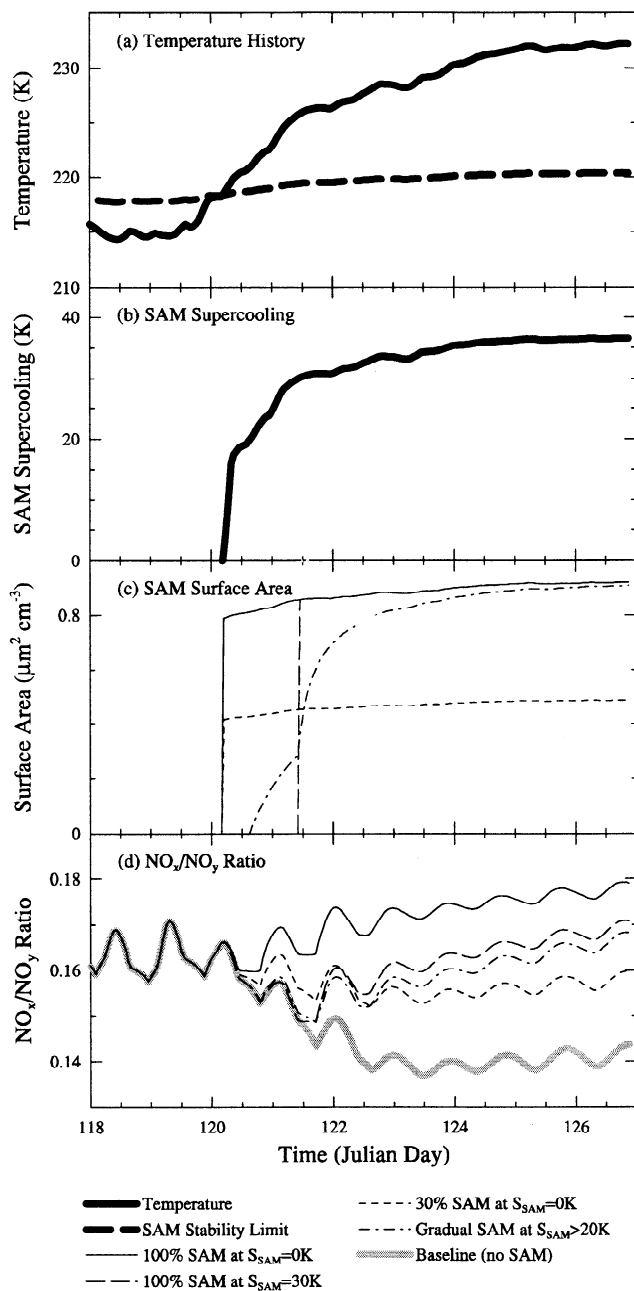


Figure 3. Evolution of a sample air parcel, demonstrating possible SAM formation scenarios. The air parcel corresponds to the trajectory for 970506 at 75600 UT. (a) Trajectory temperature and SAM stability limit (calculated for a fixed water vapour pressure). (b) SAM supercooling, S_{SAM} (see text for details). (c) Surface area of SAM aerosols, according to several possible scenarios for SAM critical supercoolings and freezing rates. (d) Modelled NO_x/NO_y ratios (where $\text{NO}_x = \text{NO} + \text{NO}_2 + 2\text{N}_2\text{O}_5 + \text{HONO} + \text{NO}_3$) for each scenario.

Alternatively, only a fraction of the particles may freeze; the model preferentially freezes the largest particles first, so that when 30% of the number of particles is frozen, about 50% of the surface area is on frozen particles. Most homogeneous freezing processes do, however, require supercooling. Even at that point, freezing may be gradual. To represent gradual freezing, a fixed freezing rate is set once a given supercooling threshold is reached ($10^9 \text{ cm}^{-3} \text{ s}^{-1}$ at

$S_{\text{SAM}} > 20 \text{ K}$, $10^{10} \text{ cm}^{-3} \text{ s}^{-1}$ at $S_{\text{SAM}} > 30 \text{ K}$). The probability of an individual particle freezing is calculated by multiplying its volume by the freezing rate [Drdla, 1996]. The freezing rates were chosen to require about ten days at $S_{\text{SAM}} > 20 \text{ K}$ and two days at $S_{\text{SAM}} > 30 \text{ K}$ for the majority of the aerosols to freeze. Slower freezing timescales cannot be properly evaluated with trajectories limited to ten days in length. Even this scenario is a crude approximation of the actual freezing microphysics, but is sufficient to evaluate how SAM formation would affect the nitrogen chemistry.

The surface area of SAM particles is predicted to be very similar to that of the liquid sulphuric acid solutions. The particle mass decreases on freezing, by up to 17%, owing to loss of excess water. Volume growth is not possible because all the H_2SO_4 is already in the condensed phase in the middle stratosphere. Even in a case where only a fraction of the particles freezes, the SAM particles cannot grow at the expense of the liquids because H_2SO_4 vapour pressures are too low to allow efficient mass transfer; this differs from the situation in cirrus clouds, for example, where higher water vapour pressures allow efficient mass transfer.

This negligible change in aerosol surface area limits the techniques available to directly detect SAM formation. Without a statistically significant change in the aerosol size distribution, optical aerosol counters cannot distinguish the phase change. The low backscatter ratios associated with background aerosol limit the sensitivity of lidar to changes in depolarization; highly aspherical particles would need to be produced for an observable depolarization signal. Therefore, specialized detection techniques may be necessary to conclusively determine whether SAM is present.

This study has instead focussed on the effect of SAM formation on heterogeneous chemistry. N_2O_5 hydrolysis decreases by two orders of magnitude, from 0.1 to 0.001, when sulphuric acid aerosols freeze into SAM [Zhang *et al.*, 1995]. In turn, the NO_x/NO_y ratio responds (Figure 3d). (In this figure only, NO_x includes NO , NO_2 , N_2O_5 , NO_3 , and HONO to minimize the diurnal cycle.) In the baseline model, the NO_x/NO_y ratio decreases in response to the temperature increase. Aerosol freezing causes the NO_x/NO_y ratio to increase relative to the baseline case, with the extent of the increase proportional to the surface area of the frozen particles.

4.1. Effect of SAM Formation on 970506

The increase in the calculated NO_x/NO_y ratio due to SAM formation can cause substantial improvement between the model and the measurements, as shown in Figure 4 for the flight of May 6th. The baseline model, in which all particles are liquid solutions, underpredicts the measurements by about 30% on this date. Assuming all the particles freeze at $S_{\text{SAM}} = 0 \text{ K}$ increases the NO_x/NO_y ratio to values very close to the measurements, along the entire flight. Even in two dives, at 73000 and 77000 UT, the model agreement is noticeably improved, with little variation in the NO_x/NO_y ratio across the first dive, but a slight variation during the second dive. The improvement in the calculated NO_x/NO_y ratio depends, however, on complete particle freezing at low SAM supersaturations. The various sensitivity tests all reduced the magnitude of the NO_x/NO_y impact.

Comparisons with other measured quantities (ClO , OH , and HO_2) also show good agreement. The greatest discrepancy is with OH (Figure 4c), which is underpredicted by on average 20% for SAM formation. Low modelled OH concentrations are a prevalent feature of POLARIS, especially for models that reproduce NO_x/NO_y ratios [Wennberg *et al.*, 1999]. The tendency of models to

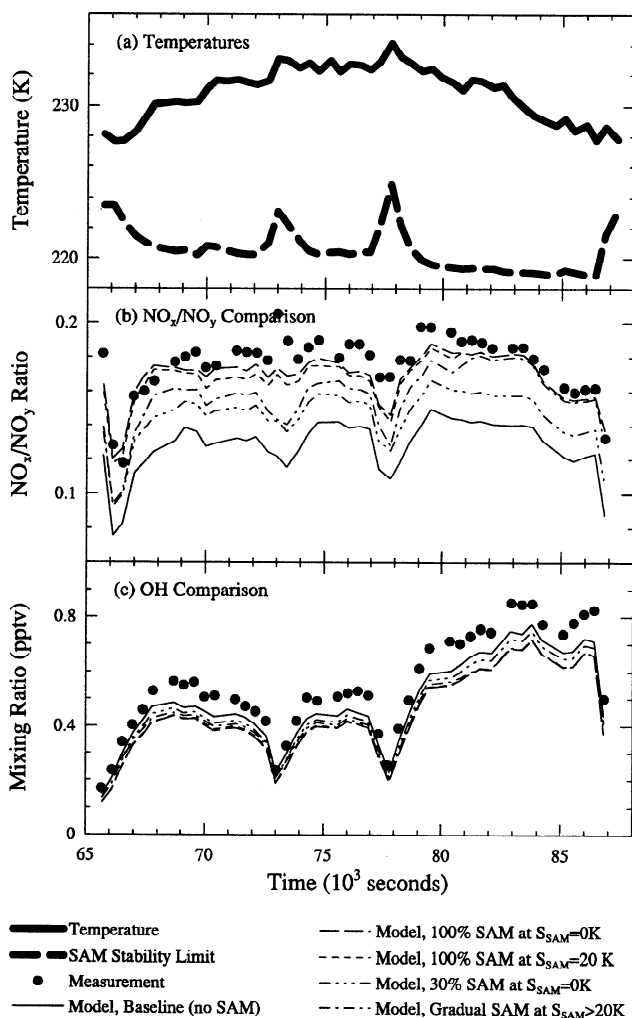


Figure 4. Model/measurement comparison along the flight of 970506 for several SAM formation scenarios. (a) Measured temperature and calculated SAM stability limit. (b) $(\text{NO}+\text{NO}_2)/\text{NO}_y$ ratios, both measured and modelled. (c) OH mixing ratios, measured and modelled.

underestimate measured NO_x and NO using standard chemistry leads to an improper overestimate of the HO_2/OH ratio; models that force agreement with measured NO_x (or NO) tend to calculate uniformly lower HO_x values for most of POLARIS.

This flight is one of the best dates for model agreement when SAM is included. The overall impact of SAM formation is assessed in Figure 5, which should be compared to the baseline case in Figure 2. Also, Table 2 presents average model/measurement comparisons for each flight. These results show the maximum possible NO_x/NO_y effect due to SAM, i.e. for the scenario with 100% freezing at $S_{\text{SAM}} = 0\text{K}$.

The effect of SAM is greatest at low NO_x/NO_y ratios; at values up to ~ 0.1 , SAM formation increases modelled NO_x/NO_y by up to 50%. This large effect tends to cause model overprediction, and the scatter is increased. The ASHOE/MAESA flights provide particularly stringent constraints on SAM freezing probabilities. Baseline simulations of these dates agreed well with measurements, but the flights also experienced the warmest temperatures of the whole database. Therefore, extensive SAM formation is predicted, with resultant overprediction of the NO_x/NO_y ratio. Especially on 941016, more than 90% of the particles must remain liquid past

supercoolings of 35 K, in order to maintain model/measurement agreement. One alternative explanation would be a slow freezing rate ($<10^9\text{ cm}^{-3}\text{ s}^{-1}$), since the extremely warm temperatures only occurred within the last two days.

However, at high NO_x/NO_y ratios SAM formation has a distinctly smaller impact. The 12% increase in NO_x levels at high values is less than necessary to match the measurements; the model underprediction at high NO_x/NO_y ratios is in strong contrast to the overprediction at low NO_x/NO_y ratios. The different behaviour can be attributed to the continuous solar exposures necessary to allow elevated NO_x/NO_y ratios. Without the usual diurnal cycle, N_2O_5 is not able to form at night and transform NO_x species back to HNO_3 . Therefore, reaction (R1) plays an increasingly small role even in the baseline case, and turning off this reaction has a small effect.

4.2. Effect of SAM Formation on 970430: The $\text{BrONO}_2+\text{H}_2\text{O}$ Reaction

The effect of SAM freezing on heterogeneous reactions besides N_2O_5 and ClONO_2 hydrolysis needs to be evaluated. In particular, the other reaction of importance on liquid aerosols at these temperatures, namely BrONO_2 hydrolysis (reaction (R2)) has not been measured on SAM. The effect of this reaction is primarily apparent at sunrise when the HOBr product, after building up overnight, photolyzes and produces a burst of OH [Hanson and Ravishankara, 1995; Lary *et al.*, 1996]. During POLARIS, sunrise measurements of OH were made on the flight of 970430, in conjunction with SAM supercoolings of 30 K. As with the flight of 970506, if SAM freezing is assumed to occur, NO_x/NO_y model/measurement agreement is improved (Figure 6b).

Figure 6c shows that OH levels are sensitive to the value used for the reaction probability of BrONO_2 on SAM. If this reaction is assumed to be inefficient ($\gamma=10^{-4}$), the model severely underpredicts OH, in particular at the zenith angles near 90° , where HOBr photolysis is most effective. However, for a reactivity of 0.8, OH levels very similar to the baseline case are predicted. The

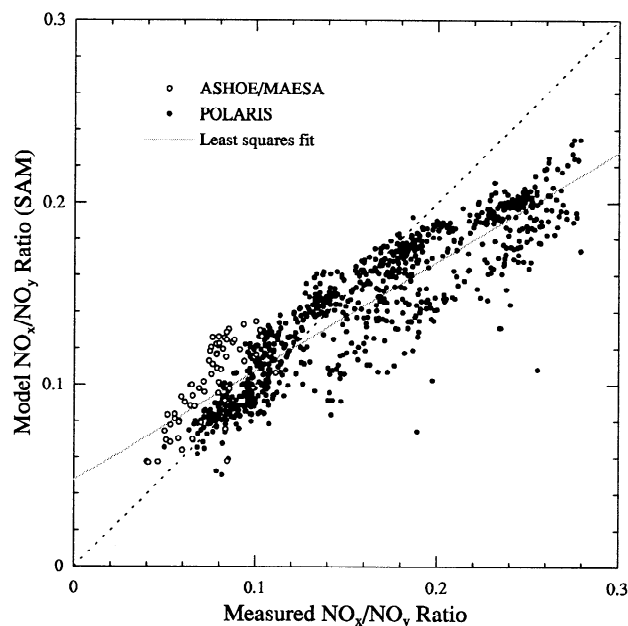


Figure 5. Cross plot of modelled and measured NO_x/NO_y ratios, for simulations in which 100% freezing to SAM occurs at $S_{\text{SAM}} = 0\text{K}$. Other details are as for Figure 2.

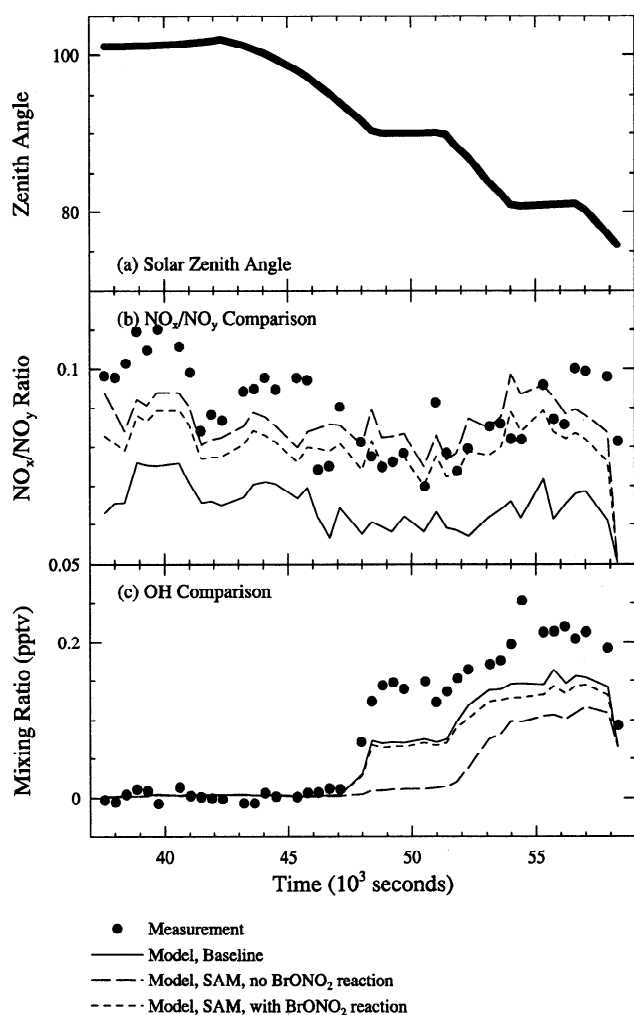


Figure 6. Model/measurement comparison along the flight of 970430, a sunrise flight, for several SAM formation scenarios. (a) Solar zenith angles. (b) $(\text{NO}+\text{NO}_2)/\text{NO}_y$ ratios, measured and modelled. (c) OH mixing ratios, measured and modelled.

remaining model/measurement discrepancy is a problem shared by other models [Wennberg *et al.*, 1999]. Uncertainties in the HOBr cross section at long wavelengths and in the Br_y budget may be partly responsible, but a full explanation of OH levels, at sunrise and through the day, is still under investigation [Wennberg *et al.*, 1999]. A further complication is that even for liquid sulphate aerosols, the assumed model reactivity of 0.8 exceeds laboratory measurements for these sulphate solutions (near 77 wt %): Hanson *et al.* [1996] found that at weight percents above 70, the reaction probability decreased. Sensitivity tests (not shown) have been performed in which γ_{BrONO_2} was calculated according to equation (4) of Hanson *et al.* [1996]; at zenith angles near 90°, a 75% decrease in OH (relative to the baseline case) resulted. Clearly our understanding of the BrONO₂ hydrolysis reaction and its role in stratospheric chemistry is not yet complete.

5. Liquid Aerosol Reactions

5.1. HONO Uptake and Reactions

Several recent studies have examined the interactions of HONO with sulphuric acid solutions [Becker *et al.*, 1996; Fenter and Rossi, 1996; Zhang *et al.*, 1996; Longfellow *et al.*, 1998]. All agree that

the uptake and solubility of HONO increase with increased solution acidity past about 55 wt %, due to HONO dissolution as a base, rather than an acid, forming NO⁺ ions (reaction (R10)) or H₂ONO⁺ ions [Longfellow *et al.*, 1998]. This dissolution has been incorporated into the model, with various treatments of the composition-dependent solubilities and uptake coefficients (Table 3). If the predicted nitrosyl sulphuric acid (NSA) solubility limit is exceeded [Burley and Johnston, 1992], NSA will precipitate out of solution, producing a mixed-phase aerosol. Furthermore, two HONO reactions, (R8) and (R9) have been incorporated into the model.

Adding just HONO dissolution to the model (scenario A1, Table 4), has negligible effects, mainly because of the low predicted concentrations of HONO. HONO mixing ratios are at most 1 pptv, so that HONO concentrations in the solution are less than 0.001 wt %, well less than the NSA saturation limit in the solutions and too small to possibly be detected in the aerosols. Furthermore, gas-phase HONO is not affected because less than 0.01% of the HONO dissolves. Similarly negligible results are obtained using the Becker *et al.* [1996] solubilities.

Both reactions (R8) and (R9) are limited by HONO availability. Even assuming a HONO reaction probability of one, these reactions are of no importance, as evaluated in scenarios A3 and A4 (not shown). The most significant effect, in scenario A4, is a 0.4% increase in the ClONO₂/HCl ratio. More realistic treatment of reaction (R9), either using limited HONO uptake [Becker *et al.*, 1996; Zhang *et al.*, 1996], or determining the reaction rate based on aqueous concentrations [Longfellow *et al.*, 1998], results in a ten-fold decrease in the reaction rate.

5.2. CH₂O Uptake and Reactions

Formaldehyde uptake by sulphuric acid solutions has been shown to be a complex process. Initial equilibration involves the formation of several possible solutes, including CH₂(OH)₂, HOCH₂⁺, and possibly HOCH₂OSO₂(OH), depending upon the acidity of the solution [Jayne *et al.*, 1996; Iraci and Tolbert, 1997]. Long-term irreversible uptake of formaldehyde is then possible, owing to formation of short-chain polymers [Iraci and Tolbert, 1997].

Methane oxidation chemistry is part of the model's standard photochemistry, leading to formaldehyde mixing ratios of ~20 pptv at ER-2 altitudes. Thus the CH₂O pressure is three orders of magnitude lower than those used in the formaldehyde polymerization study of Iraci and Tolbert [1997]. Although the reaction kinetics for polymerization in solution were not determined, linear scaling from the laboratory timescales (10³ s) would suggest that at least 10⁶ s are necessary for polymerization; a second-order reaction is more likely and would require even longer timescales. Furthermore, reaction with HNO₃ (reaction 7) will compete with polymerization. Therefore, CH₂O polymerization reactions have not been included in the model.

Instead, CH₂O uptake is simply treated with an effective Henry's law solubility of 10⁷ M/atm, at the high end of measurements [Iraci and Tolbert, 1997]. Even with this solubility, the condensed phase concentration is limited to 10⁻⁵ wt %.

Reaction with HNO₃ is incorporated using the parameters in Table 3. The most important parameter controlling this reaction rate is the formaldehyde uptake. The probability of CH₂O reaction with HNO₃, i.e., $\gamma_{\text{CH}_2\text{O}}$, has not been measured; only the CH₂O uptake coefficient (in the absence of HNO₃) has been measured. Laboratory data shows that the CH₂O uptake coefficient decreases rapidly with time, owing to CH₂O equilibration with the solution [Tolbert *et al.*, 1993; Jayne *et al.*, 1996; Iraci and Tolbert, 1997].

However, under stratospheric conditions, the model results show that formaldehyde is efficiently removed from the solution by reaction (R7). Therefore, the relevant uptake coefficient should be the initial one, i.e., for a solution with minimal CH_2O . This value is not well constrained in existing laboratory studies [Jayne *et al.*, 1996]. In this study, two CH_2O reactive probabilities have been tested. First, to demonstrate the maximum possible effect of this reaction, and thus determine whether further study is warranted, a reactive probability of one was used in most model runs. For a more realistic estimate, the uptake coefficients measured by Tolbert *et al.* [1993] on stirred solutions at 223 K were used in a second set of simulations. Even in this scenario, the diffusion of HNO_3 to the particles far exceeds CH_2O uptake, so that all CH_2O uptake leads to reaction. Therefore, the CH_2O uptake coefficient will be treated as its reactive probability in this study.

The HNO_3 reaction probability is based on the only available measurement, namely the lower limit of 0.01 estimated by Iraci and Tolbert [1997] for a 90 wt % sulfuric acid solution. This value of 0.01 was assumed to be applicable for all conditions in this study. As just mentioned, however, CH_2O uptake always limits the reaction rate, preventing the simulation from being sensitive to γ_{HNO_3} . Effective HNO_3 reaction probabilities, taking into account formaldehyde availability, are at least a factor of two smaller.

The effects of this reaction alone, scenarios B1 and B2, are shown in Figure 7. Multiple direct effects are predicted, including increases in the NO_x/NO_y ratio, increases in HONO and thus HO_x , perturbations to the formaldehyde chemistry, and production of a new species, formic acid (CHOOH). Each of these effects, and factors influencing their magnitude, will be discussed individually.

The most important effect of this reaction is conversion HNO_3 to NO_x , increasing the NO_x/NO_y ratio by up to 20% overall (for

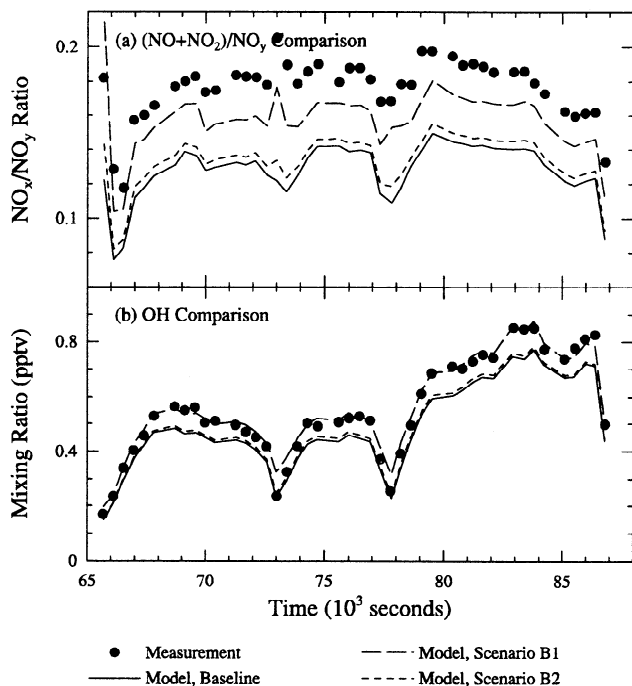


Figure 7. Model/measurement comparison along the flight of 970506, when reaction (R7), $\text{CH}_2\text{O}+\text{HNO}_3$, is included, using either $\gamma_{\text{CH}_2\text{O}}=1$ (scenario B1) or a parameterization of $\gamma_{\text{CH}_2\text{O}}$ based on Tolbert *et al.* [1993] (scenario B2). (a) $(\text{NO}+\text{NO}_2)/\text{NO}_y$ ratios, measured and modelled. (b) OH mixing ratios, measured and modelled.

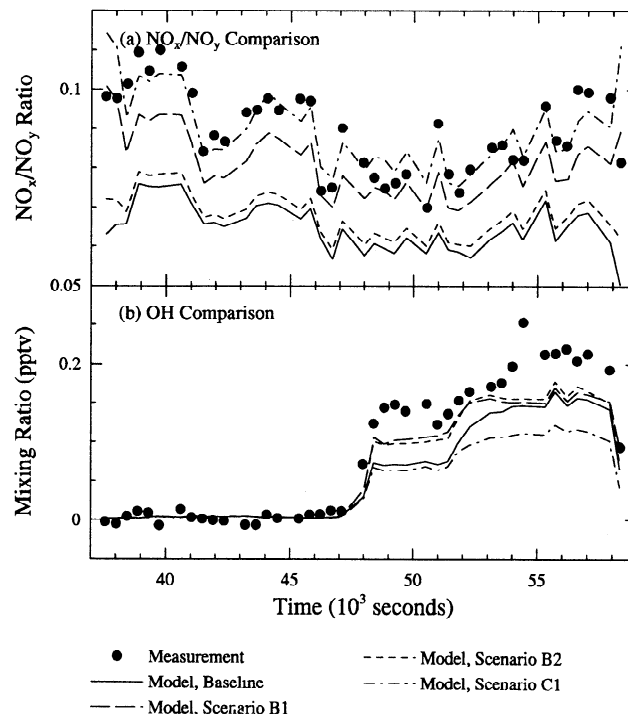


Figure 8. Model/measurement comparison along the flight of 970430, a sunrise flight, when reaction (R7), $\text{CH}_2\text{O}+\text{HNO}_3$, is included, using either $\gamma_{\text{CH}_2\text{O}}=1$ (scenario B1) or a parameterization of $\gamma_{\text{CH}_2\text{O}}$ based on Tolbert *et al.* [1993] (scenario B2). Also shown are results for all reactions (R1)–(R9) with $\gamma_{\text{CH}_2\text{O}}=1$ (scenario C1). (a) $(\text{NO}+\text{NO}_2)/\text{NO}_y$ ratios, measured and modelled. (b) OH mixing ratios, measured and modelled.

scenario B1). Unlike SAM formation, this reaction is somewhat more effective during continuous solar exposure, since photochemical production of formaldehyde limits the reaction rate, especially for $\gamma_{\text{CH}_2\text{O}}=1$.

That the NO_x product is HONO has several implications. First, HONO is also a source of HO_x . Therefore a net increase in OH is predicted (Figure 7b), even though the NO_x increase is acting to decrease HO_x levels (as seen, for example, in Figure 4c). The effect on HO_x is especially apparent for sunrise conditions, demonstrated by the flight of 970430 (Figure 8). Predicted OH values for solar zenith angles of 90° approach the measurements; furthermore, the morning OH levels are almost insensitive to the assumed value of $\gamma_{\text{CH}_2\text{O}}$. HONO photolysis is responsible for the OH burst in this scenario, as originally proposed by Salawitch *et al.* [1994b], although from a different heterogeneous reaction. This OH source could provide an alternative explanation for hydroxyl model/measurement discrepancies during POLARIS. However, as discussed by Wennberg *et al.* [1999] and confirmed by simulations (not shown) using scenario B1 for two POLARIS sunset flights, a limitation of a HONO mechanism is that the photolysis of HONO at even higher solar zenith angles ($>90^\circ$) is too slow to explain sunset measurements of OH and HO_2 .

The second effect of producing HONO is to greatly increase HONO (and NO^+) concentrations in the condensed phase. The gas-phase increase in HONO, by a factor of ten, increases the equilibrium aqueous HONO concentration by the same magnitude. In addition, aqueous HONO levels in excess of equilibrium are predicted by the model. The model solves for the steady state aqueous concentration, $[\text{HONO}]_{\text{aq}}$ necessary to balance the HONO

sources (heterogeneous production, P_{het} , and HONO diffusion to the particle, P_{diff}) with HONO loss due to transport away from the particle (L):

$$P_{\text{het}} + P_{\text{diff}} - L = 0 \quad (1a)$$

or

$$P_{\text{het}} + 4\pi rD[\text{HONO}]_{g,\infty} - 4\pi rD[\text{HONO}]_{aq}H^*RT = 0 \quad (1b)$$

where r is the particle radius (cm), D is the diffusivity of HONO (incorporating particle size adjustments, cm^2/s), $[\text{HONO}]_{g,\infty}$ is the ambient gas-phase HONO concentration (cm^{-3}), H^* is the effective Henry's law coefficient for HONO, R is the gas constant, and T is the temperature. Note that in the case of no heterogeneous production, this equation is equivalent to the diffusion equation, with $[\text{HONO}]_{aq}$ calculated according to Henry's law. However, if the reaction of CH_2O is efficient, the HONO production rate is an order of magnitude faster than the rate of HONO diffusion to the particle. To balance this production, the aqueous HONO concentration increases, permitting more rapid evaporational and diffusional loss from the particle surface. Equation (1) provides a method of estimating the magnitude of that increase, in the case of $\gamma_{\text{CH}_2\text{O}}=1$ predicting that the aqueous concentration is enhanced relative to equilibrium by about a factor of ten. However, even with this net two orders of magnitude enhancement in aqueous HONO concentrations (relative to simulations without reaction (R7)), the maximum HONO weight percent is still more than a thousand times smaller than the NSA solubility limit. Other implications of aqueous-phase HONO production, in particular possible heterogeneous chemistry, will be discussed in section 5.3.

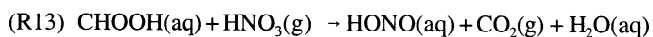
The other reaction product is formic acid, a species not otherwise predicted to be present appreciably in the stratosphere. Oxidation of formic acid by OH is slow [DeMore *et al.*, 1997]. Other gas-phase CHOOH sinks, for example reaction with Cl [Wallington *et al.*, 1990] or photolysis [Calvert and Pitts, 1966; Wine *et al.*, 1985], are orders of magnitude slower than the OH reaction in the lower stratosphere. As a result, CHOOH builds up to high levels: equilibrium concentrations of formic acid are calculated to be 3 to 4 ppbv for $\gamma_{\text{CH}_2\text{O}}=1$. About one month would be necessary for these concentrations to be reached; over the ten-day trajectories used here, the concentration only reaches 0.8 ppbv for $\gamma_{\text{CH}_2\text{O}}=1$.

Another potential sink for formic acid is the aqueous-phase "Morgan reaction" [Smith *et al.*, 1983]:



In scenario B3 this process was included in the model (Table 4). Only minor depletion of CHOOH was calculated; a six order of magnitude increase in either the rate or the solubility was necessary to limit equilibrium CHOOH levels to 200 pptv. A limited efficiency for this reaction is consistent with a reactive uptake of at most 0.05 as determined by Klassen *et al.* [1997].

Another possibility is the further reaction of CHOOH with HNO_3 :



This aqueous phase reaction has been documented in nitric acid solutions [Horváth *et al.*, 1988] but was at least an order of magnitude slower than the reaction of formaldehyde with HNO_3 . Reaction (R13) has been tested using an HNO_3 reaction probability of either 0.01 (scenario B4) or 0.0005 (scenario B5). If $\gamma_{\text{HNO}_3} \geq 0.01$, the reaction rate is limited only by CHOOH production. HNO_3 consumption and thus all predicted effects of reaction (R7) are effectively doubled. Since all CHOOH is consumed, formic acid

does not build up in the gas phase. However, $\gamma_{\text{HNO}_3}=0.0005$ may be more realistic, causing reaction (R13) to be about ten times slower than reaction (R7), in accordance with Horváth *et al.* [1988]. In this case, reaction (R13) has a moderate effect on NO_x activation levels (10% more HNO_3 is consumed than in scenario B1); equilibrium CHOOH levels are reduced by 20% but are still at ppbv levels.

In summary, while stratospheric sinks for formic acid have not been fully explored, it seems likely that reaction (R7) will lead to much higher levels of formic acid than would otherwise be predicted. Even using Tolbert's $\gamma_{\text{CH}_2\text{O}}$ values (scenario B2), equilibrium CHOOH levels are 0.5 ppbv. Stratospheric measurements of CHOOH should therefore provide a stringent test for the occurrence of reaction (R7).

Finally, reaction (R7) is also an efficient sink of formaldehyde. The most obvious effect is a 40% decrease in modelled CH_2O for $\gamma_{\text{CH}_2\text{O}}=1$; a diurnal cycle is also introduced, whereas in the baseline model there are no nighttime formaldehyde sinks. This perturbation to the formaldehyde chemistry has implications for the stratospheric hydrogen budget. In the methane oxidation cycle, the pathway of CH_2O degradation determines whether CH_4 is ultimately converted to two H_2O molecules or to H_2O and H_2 . Hurst *et al.* [1999] have shown that with gas-phase chemistry, the ratio of H_2O production (by CH_4 and H_2 oxidation) to CH_4 loss is 1.97, which is at the low end of the range observed by several in situ measurements, 2.15 ± 0.18 . The formic acid produced by reaction (R7) should ultimately yield H_2O , whether via reaction (R12), (R13), or reaction with OH. Thus, this reaction will tend to increase H_2O production; in these calculations the H_2O yield from CH_2O degradation alone increases from 40-45% to 70-85%. However, methane oxidation is efficient at altitudes extending above the sulphate layer. Evaluation of the overall impact of reaction (R7) on methane oxidation will require calculations in a two- or three-dimensional stratospheric model.

5.3. Combined Effects of Reactions (R7), (R8), and (R9)

By creating aqueous phase HONO, the formaldehyde reaction provides a new pathway for the HONO reactions, (R8) and (R9). In particular, since the HONO is created in the aqueous phase, the rates of these reactions are no longer sensitive to HONO diffusion or uptake. To model these reactions, we have assumed that all HONO created by reaction (R7) will react with any available HCl or HNO_3 (based on γ_{HCl} and γ_{HNO_3}); HONO will only desorb to the gas phase if insufficient HCl and/or HNO_3 are available for secondary reactions. This assumption is supported by the measured affinity of HONO for sulphuric acid solutions and the aqueous-phase enhancement of HONO predicted by equation (1).

The relative efficiency of HCl versus HNO_3 reaction is determined in the model by the relative uptakes of these two species, taking into account gas-phase concentrations, diffusivities, and uptake coefficients. For scenarios C1 and C2, reaction with HNO_3 is favoured by about 2:1 using this formulation. However, note that γ_{HNO_3} is only a lower limit estimated by Iraci and Tolbert [1997] for HNO_3 reaction with CH_2O , rather than with HONO, and therefore can be considered to have a large uncertainty. Also, according to Longfellow *et al.* [1998], γ_{HCl} is orders of magnitude smaller under these conditions than the 0.02 assumed here; a continued decrease in the HCl solubility with solution acidity would further limit the HCl reactivity (since the Longfellow *et al.* [1998] data is for 70 wt % solutions). Given these uncertainties, runs have also been done with reactions (R8) and (R9) separately, to examine the sensitivity to the relative efficiencies of these pathways.

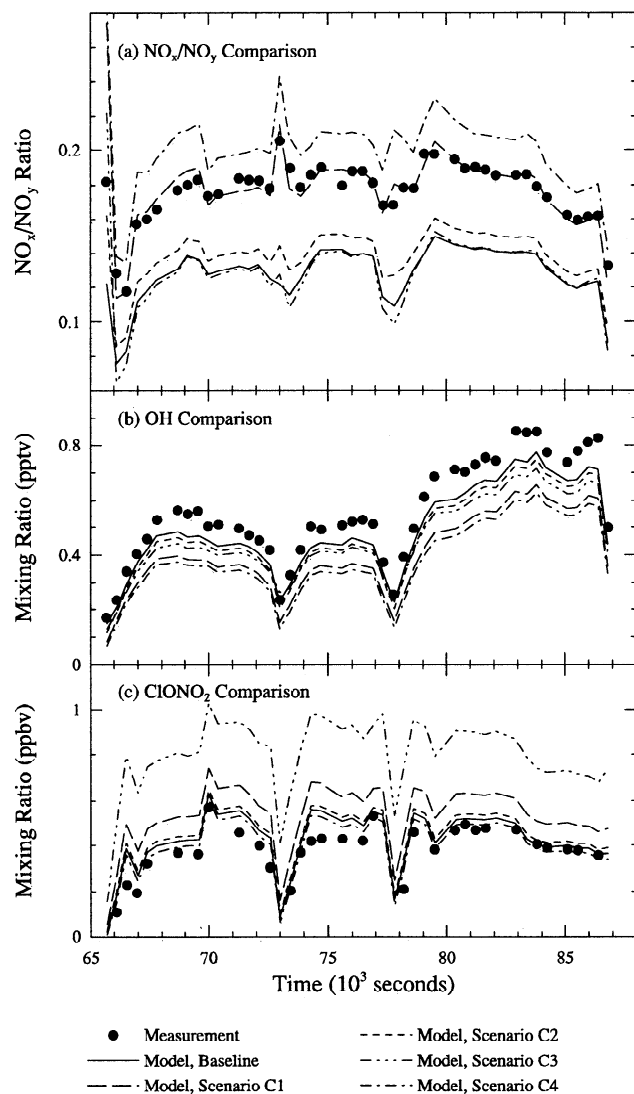


Figure 9. Model/measurement comparison along the flight of 970506, when reaction (R7) ($\text{CH}_2\text{O}+\text{HNO}_3$) is combined with reaction (R8) ($\text{HONO}+\text{HCl}$) and/or reaction (R9) ($\text{HONO}+\text{HNO}_3$). In most cases $\gamma_{\text{CH}_2\text{O}}=1$; one simulation (scenario C2) is shown using *Tolbert et al.* [1993] values for $\gamma_{\text{CH}_2\text{O}}$. See Table 4 for a full description of each scenario. (a) $(\text{NO}+\text{NO}_2)/\text{NO}_y$ ratios, measured and modelled. (b) OH mixing ratios, measured and modelled. (c) ClONO_2 mixing ratios, measured and modelled.

The further reaction of HNO_3 with HONO enhances the effect on NO_x/NO_y ratios (Figure 9a), to the point where values are overall very similar to the measurements if $\gamma_{\text{CH}_2\text{O}}=1$. Higher resolution NO_x/NO_y data even show a "spike" analogous to the model in the dive at 73000 UT. This agreement can also be seen in Figure 10a for all the simulated flights, where the model/measurement least squares fit is very near the one-to-one line. This demonstrates that these liquid reactions can be effective over a wide range of conditions, unlike N_2O_5 hydrolysis, which becomes less effective during the continuous solar exposure of polar summer. In fact, the $\text{CH}_2\text{O}+\text{HNO}_3$ reaction becomes somewhat more effective during polar summer, because of the 24-hour production of formaldehyde. However, the overall scatter of the modelled points has increased, especially at the high values of NO_x/NO_y . Individual points in

Figure 10a are far above the one-to-one line; for nine points, modelled NO_x/NO_y even exceeded 0.3. And the increase in modelled NO_x/NO_y levels extends to the ASHOE/MAESA flights, worsening the initially favourable model/measurement agreement. Therefore $\gamma_{\text{CH}_2\text{O}}=1$, which is probably unrealistically large based on aerosol chemistry alone, is also too large to be consistent with NO_x/NO_y chemistry. Any further HNO_3 processing via reaction (R13) (which was not included in scenario C1) or changes in the gas-phase reaction rates [*Brown et al.*, 1999a, b; *Dransfield et al.*, 1999] would exacerbate the problem.

For a more conservative value of $\gamma_{\text{CH}_2\text{O}}$, a more moderate effect is of course predicted (Figure 10b); overall NO_x/NO_y levels increase by 8% if *Tolbert et al.* [1993] reaction probabilities are assumed (scenario C2). A net 12% increase is predicted if only reactions (R7) and (R8) are included (scenario C5, not shown); a 24% increase is possible if reaction (R13) is also efficient (scenario C6,

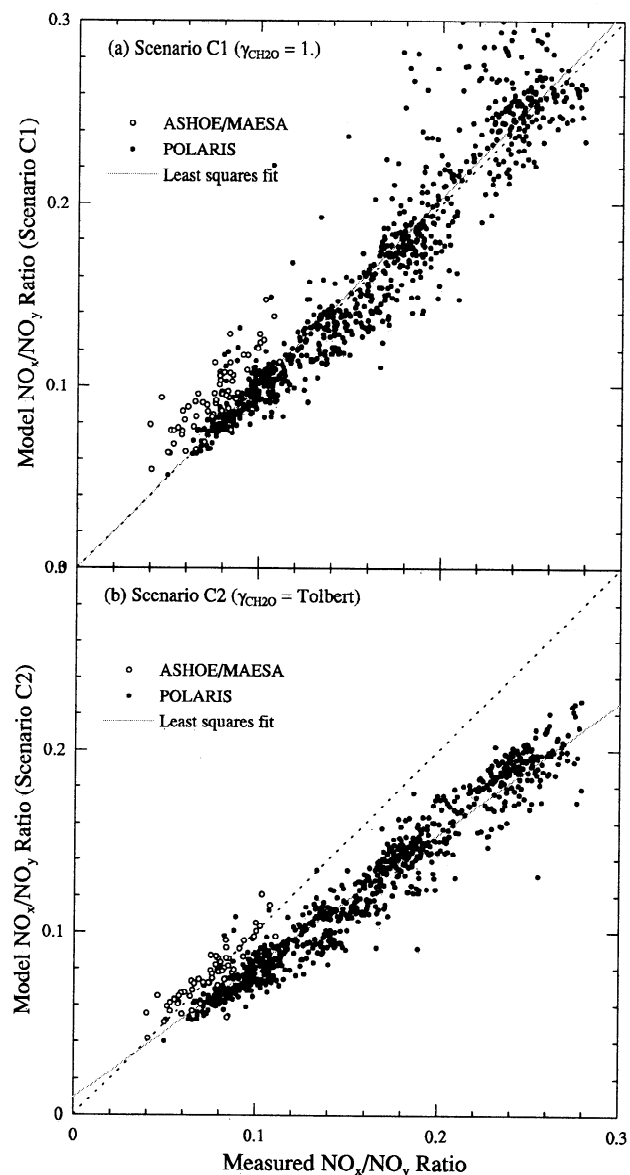


Figure 10. Cross plot of modelled and measured NO_x/NO_y ratios, for simulations in which reactions (R7), (R8), and (R9) are all included. (a) $\gamma_{\text{CH}_2\text{O}}=1$ (scenario C1). (b) $\gamma_{\text{CH}_2\text{O}}$ is derived from *Tolbert et al.* [1993] (scenario C2). Other details are as for Figure 2.

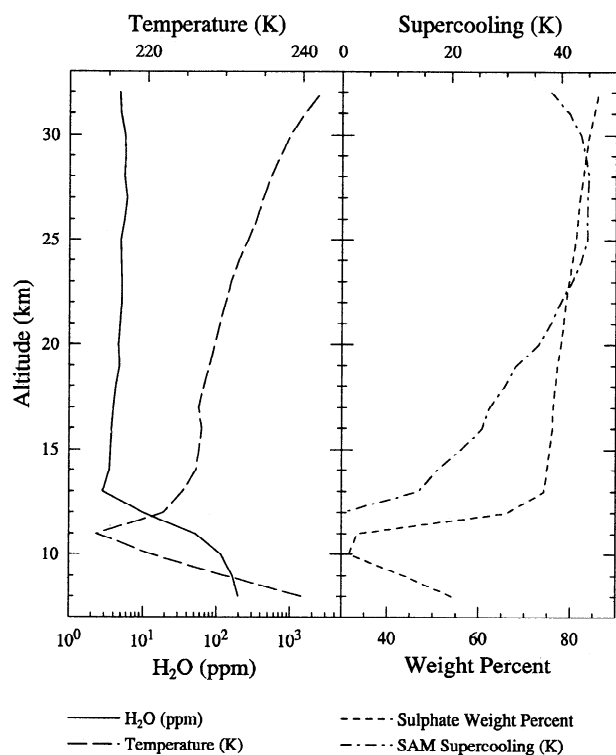


Figure 11. (a) MkIV temperature and water profile [Toon *et al.*, this issue], measured over Fairbanks, Alaska, on July 8, 1997. (b) Sulphate composition and SAM supercooling calculated from the measurements.

not shown). Therefore, formaldehyde activation of HNO₃ can influence stratospheric NO_x/NO_y partitioning even using a moderate value for $\gamma_{\text{CH}_2\text{O}}$, demonstrating that further research into this reaction is warranted.

Including the secondary HONO reactions (R8) and (R9) eliminates the release of HONO to the gas phase, so a positive effect on HO_x is not longer predicted. Instead, the NO_x increase promotes an indirect 20% decrease in OH (Figure 9b), worsening agreement with the measurements. This effect was also shown for sunrise conditions in Figure 8b, where the morning OH release is diminished overall once the secondary reactions (R8) and (R9) were included. Thus, improvements in model predictions of OH are only possible via reaction (R7) if most of the HONO does desorb from the aqueous phase.

The reaction of HONO and HCl causes a 20 to 50% increase in ClONO₂, at the expense of HCl (Figure 9c), which worsens model comparisons to ClONO₂ measurements. This result, however, is particularly sensitive to the relative partitioning between reactions (R8) and (R9). The results in which HONO exclusively reacts with HCl (scenario C3) have dramatic effects on chlorine partitioning, which cause the model to far exceed measurements of ClONO₂ and ClO (not shown). This extreme chlorine activation in turn negatively impacts the NO_x/NO_y ratio, by removing NO₂ to ClONO₂. Even using the slower Tolbert uptake coefficients for CH₂O (scenario C7), 10% changes in the ClONO₂/HCl ratio are predicted if HONO+HCl is the sole secondary reaction. In another test (scenario C8, not shown), the Longfellow *et al.* [1998] parameterization was used, instead of a constant $\gamma_{\text{HCl}}=0.02$. This resulted in a ten-fold decrease of the reaction rate, and eliminated the unrealistic chlorine activation. These results suggest that

reaction with HNO₃ is favoured over reaction with HCl by more than the 2:1 ratio assumed by the default reaction probabilities.

At the other extreme, complete reaction of the HONO with HNO₃ can cause continued increases in the NO_x/NO_y ratio. For $\gamma_{\text{CH}_2\text{O}}=1$, this increase drives the model values past the measurements which is probably unrealistic. However, for the lower CH₂O reaction probability (scenario C5), this changes the overall effect on NO_x/NO_y ratios to 12%, as mentioned earlier in this section.

6. Altitude Dependence

This analysis focussed on ER-2 data because of the availability of a wide range of simultaneous measurements. However, many of the processes discussed in this paper would be more effective at higher altitudes. Figure 11a shows profiles of temperature and H₂O retrieved by the MkIV balloon-borne instrument during a flight from Fairbanks on 970708, in conjunction with the POLARIS campaign [Toon *et al.*, this issue]. The sulphuric acid weight percent and SAM supercooling calculated from this water and temperature profile are shown in Figure 11b. Both values clearly increase with altitude, because of both the increase in temperature and the decrease in water partial pressure. Climatological data shows the same temperature trend with altitude [Rosenlof, 1996].

Also evident in this plot is that the upper troposphere is too moist for highly concentrated sulphuric acid solutions. Therefore, we expect that acid-catalysed reactions will be more effective in the stratosphere than the troposphere, although several studies have proposed a role for these reactions in the troposphere.

7. Conclusions

We have done an initial analysis of the potential for alternative theories of sulphate aerosol composition and chemistry to affect our understanding of stratospheric chemistry at warm stratospheric temperatures. The processes we investigated, including sulphuric acid monohydrate formation, formaldehyde activation of HNO₃, and secondary reactions of the HONO product, have not previously been included in models, in part because they are poorly understood. However, these processes have been shown to have effects in our photochemical model that are large enough to warrant further study.

In particular, reaction (R7) of formaldehyde and HNO₃ [Iraci and Tolbert, 1997] favourably affects model predictions of NO_x/NO_y ratios and OH concentrations. The HONO produced by the formaldehyde reaction in turn promotes secondary reactions of HNO₃ [Iraci and Tolbert, 1997] and HCl [Zhang *et al.*, 1996; Longfellow *et al.*, 1998], which otherwise would not be effective in the stratosphere. Using realistic CH₂O uptake coefficients (0.015-0.12, as measured by Tolbert *et al.* [1993]), an 8-24% increase in NO_x/NO_y is predicted, depending upon the extent of secondary reaction. OH enhancements in agreement with measurements are predicted both during the day and at sunrise, if HONO from reaction (R7) is released to the gas phase. However, the data suggest a limited role for the reaction of HCl with HONO, because this reaction would activate chlorine and increase ClONO₂/HCl ratios past observed values if Zhang *et al.* [1996] reactivities are used; much less chlorine activation is predicted, however, using the Longfellow *et al.* [1998] reactivities, supporting their lower values. One conclusive indicator of the formaldehyde reaction may be formic acid, which is predicted to reach gas-phase mixing ratios in excess of 0.5 ppbv. Even more extreme effects

are shown to be theoretically possible if the CH_2O reactivity is increased.

Further laboratory data on several aspects of these reactions are necessary to provide confidence in model results. The most important parameter is the formaldehyde reaction probability, which controls the rate of reaction (R7) in these simulations. Measurements of this parameter in the presence of HNO_3 have not been made; the only values available in the literature [Tolbert *et al.*, 1993; Jayne *et al.*, 1996; Iraci and Tolbert, 1997] are uptake coefficients measured after CH_2O had begun to dissolve in the sulphate solutions, limiting uptake. The dependence of the uptake and reactivity on sulphuric acid composition is also uncertain.

Further uncertainties relate to the fate of the products of reaction (R7). For HONO, questions include how much is released to the gas phase and the relative efficiencies of reactions (R8) and (R9). For example, detailed kinetic information such as Longfellow *et al.* [1998] needs to be provided for reaction (R9) ($\text{HONO} + \text{HNO}_3$) and extended to 80 wt % H_2SO_4 solutions. For CHOOH, more information on its possible sinks is needed, in particular regarding the efficiency of its reaction with HNO_3 in sulphuric acid solutions. Other organic species also become soluble in concentrated sulphate solutions (for example acetone, Duncan *et al.*, 1998); the possibility of such species reacting, in particular with HNO_3 should be considered.

However, this study suggests a lesser role for several other proposed sulphate processes. Buildup of formaldehyde polymer chains seems unlikely with the low concentrations of formaldehyde in stratospheric solutions, especially if the aqueous concentrations are limited by efficient reaction with HNO_3 . Formation of solid nitrosyl sulphuric acid (NSA) requires large aqueous phase concentrations of HONO. While reaction (R7) can enhance dissolved HONO, the largest predicted concentrations were still three orders of magnitude lower than the NSA solubility limit.

Freezing of solutions to sulphuric acid monohydrate is thermodynamically favoured but no clear evidence for its formation can be found from the chemistry. Good baseline model agreement with NO_x/NO_y ratios was found on the flights where SAM was most likely to occur; these flights imply that SAM formation requires supercoolings greater than 35 K. Furthermore, this process is not effective at influencing NO_x/NO_y ratios during continuous solar exposure, and any decrease in BrONO_2 reactivity on frozen aerosols would lead to discrepancies with morning OH production. However, higher SAM supercoolings (due to warmer temperatures and lower water vapour pressures) do occur above ER-2 altitudes; values of 45 K are predicted at 25-28 km on one sample balloon profile. Further studies at higher altitudes are warranted. Even at ER-2 altitudes, a small fraction (10%) of the aerosols could be freezing without having a pronounced effect on the chemistry. More extensive sampling in the Southern Hemisphere would also be of interest, given observations that temperatures are warmer in the Southern Hemisphere summer than in the Northern Hemisphere [Rosenlof, 1996].

Acknowledgements. The authors wish to thank the POLARIS science team for the data used in this study, with special thanks to R.J. Salawitch, R.S. Gao, and P. Wennberg for valuable input. L. Iraci, R. Chatfield, and J. Orlando all provided helpful information. This research was funded through the NASA Upper Atmosphere Research Program. KD is supported by an NRC research fellowship.

References

- Becker, K.H., J. Kleffmann, R. Kurtenbach, and P. Wiesen, Solubility of nitrous acid (HONO) in sulfuric acid solutions, *J. Phys. Chem.*, **100**, 14984-14990, 1996.
- Brown, S.S., R.K. Talukdar, and A.R. Ravishankara, Rate constants for the reaction $\text{OH} + \text{NO}_2 + \text{M} \rightarrow \text{HNO}_3 + \text{M}$ under atmospheric conditions, *Chem. Phys. Lett.*, **299**, 277-284, 1999a.
- Brown, S.S., R.K. Talukdar, and A.R. Ravishankara, Reconsideration of the rate constant for the reaction of hydroxyl radicals with nitric acid, *J. Phys. Chem. A*, **103**, 3031-3037, 1999b.
- Burley, J.D., and H.S. Johnston, Nitrosyl sulfuric acid and stratospheric aerosols, *Geophys. Res. Lett.*, **19**, 1363-1366, 1992.
- Calvert, J.G., and J.N. Pitts Jr., *Photochemistry*, John Wiley, New York, 1966.
- Del Negro, L., et al., Comparison of modeled and observed values of NO_2 and J_{NO_2} during the Polaris Ozone Loss in the Arctic Region in Summer mission, *J. Geophys. Res.*, this issue.
- DeMore, W.B., S.P. Sander, D.M. Golden, R.F. Hampson, M.J. Kurylo, C.J. Howard, and A.R. Ravishankara, C.E. Kolb, and M.J. Molina, *Chemical Kinetics and Photochemical Data for Use in Stratospheric Modeling, Evaluation Number 12, JPL Publ. 97-4*, Jct Propulsion Lab., Pasadena, Calif., 1997.
- Dransfield, T.J., K.K. Perkins, N.M. Donahue, J.G. Anderson, M.M. Sprengnether, and K.L. Demerjian, Temperature and pressure dependent kinetics of the gas-phase reaction of the hydroxyl radical with nitrogen dioxide, *Geophys. Res. Lett.*, **26**, 687-690, 1999.
- Drdla, K., Applications of a model of polar stratospheric clouds and heterogeneous chemistry, Ph.D. Thesis, Univ. of Calif. at Los Angeles, Los Angeles, 1996.
- Duncan, J.L., L.R. Schindler, and J.T. Roberts, A new sulfate-mediated reaction: Conversion of acetone to trimethylbenzene in the presence of liquid sulfuric acid, *Geophys. Res. Lett.*, **25**, 631-634, 1998.
- Elliott, S., R.P. Turco, and M.Z. Jacobson, Tests on combined projection/forward differencing integration for stiff photochemical family systems at long time step, *Comput. Chem.*, **17**, 91-102, 1993.
- Fahey, D.W., et al., In situ measurements constraining the role of sulphate aerosols in mid-latitude ozone depletion, *Nature*, **363**, 509-514, 1993.
- Farlow, N.H., D.M. Hayes, and H.Y. Lcm, Stratospheric aerosols: Undissolved granules and physical state, *J. Geophys. Res.*, **82**, 4921-4929, 1977.
- Fenter, F.F., and M.J. Rossi, Heterogeneous kinetics of HONO on H_2SO_4 solutions and on ice: Activation of HCl, *J. Phys. Chem.*, **100**, 13765-13775, 1996.
- Gable, C.M., H.F. Betz, and S.H. Maron, Phase equilibria of the system sulfur trioxide-water, *J. Am. Chem. Soc.*, **72**, 1445-1448, 1950.
- Gaines, S. (Ed.), Airborne Southern Hemisphere Ozone Experiment and Measurements for Assessing the Effects of Stratospheric Aircraft [CD-ROM], NASA Ames Research Center, Moffett Field, Calif., 1995.
- Gao, R.S. et al., A comparison of observations and model simulations of NO_x/NO_y in the lower stratosphere, *Geophys. Res. Lett.*, **26**, 1153-1156, 1999.
- Hanson, D.R., and A.R. Ravishankara, Reactive uptake of ClONO_2 onto sulfuric acid due to reaction with HCl and H_2O , *J. Phys. Chem.*, **98**, 5728-5735, 1994.
- Hanson, D.R., and A.R. Ravishankara, Heterogeneous chemistry of bromine species in sulfuric acid under stratospheric conditions, *Geophys. Res. Lett.*, **22**, 385-388, 1995.
- Hanson, D.R., A.R. Ravishankara, and S. Solomon, Heterogeneous reactions in sulfuric acid aerosols: A framework for model calculations, *J. Geophys. Res.*, **99**, 3615-3629, 1994.
- Hanson, D.R., A.R. Ravishankara, and E.R. Lovejoy, Reaction of BrONO_2 with H_2O on submicron sulfuric acid aerosol and the implications for the lower stratosphere, *J. Geophys. Res.*, **101**, 9063-9069, 1996.
- Hints, E.J., E.M. Weinstock, J.G. Anderson, R.D. May, and D.F. Hurst, On the accuracy of in situ water vapor measurements in the troposphere and lower stratosphere with the Harvard Lyman- α hygrometer, *J. Geophys. Res.*, **104**, 8183-8189, 1999.
- Horváth, M., I. Lengyel, and G. Bazsa, Kinetics and mechanism of autocatalytic oxidation of formaldehyde by nitric acid, *Int. J. Chem. Kinet.*, **20**, 687-697, 1988.
- Hurst, D.F. et al., Closure of the hydrogen budget of the northern extratropical lower stratosphere, *J. Geophys. Res.*, **104**, 8191-8200, 1999.
- Iraci, L.T., and M.A. Tolbert, Heterogeneous interaction of formaldehyde with cold sulfuric acid: Implications for the upper troposphere and lower stratosphere, *J. Geophys. Res.*, **102**, 16099-16107, 1997.
- Jayne, J.T., D.R. Worsnop, C.E. Kolb, E. Swartz, and P. Davidovits, Uptake of gas-phase formaldehyde by aqueous acid surfaces, *J. Phys. Chem.*, **100**, 8015-8022, 1996.
- Kelly, K.K., M.H. Proffitt, K.R. Chan, M. Loewenstein, J.R. Podolske, S.E. Strahan, J.C. Wilson, and D. Kley, Water vapor and cloud water measurements over Darwin during the STEP 1987 tropical mission, *J. Geophys. Res.*, **98**, 8713-8723, 1993.

- Klassen, J.K., K.M. Fehrer, and G.M. Nathanson, Collisions of organic molecules with concentrated sulfuric acid: Scattering, trapping, and desorption, *J. Phys. Chem. B*, *101*, 9098-9106, 1997.
- Koop, T., B. Luo, U.M. Biermann, P.J. Crutzen, and Th. Peter, Freezing of HNO₃/H₂SO₄/H₂O solutions at stratospheric temperatures: Nucleation statistics and experiments, *J. Phys. Chem.*, *101*, 1117-1133, 1997.
- Lary, D.J., M.P. Chipperfield, R. Toumi, and T. Lenton, Heterogeneous atmospheric bromine chemistry, *J. Geophys. Res.*, *101*, 1489-1504, 1996.
- Loewenstein, M., J.R. Podolske, and S.E. Strahan, Atlas instrument characterization: Accuracy of the AASE and AAOE nitrous oxide data sets, *Geophys. Res. Lett.*, *17*, 481-484, 1990.
- Longfellow, C.A., T. Imamura, A.R. Ravishankara, and D.R. Hanson, HONO solubility and heterogeneous reactivity on sulfuric acid surfaces, *J. Phys. Chem. A*, *102*, 3323-3332, 1998.
- May, R.D., Open-path, near-infrared tunable diode laser spectrometer for atmospheric measurements of H₂O, *J. Geophys. Res.*, *103*, 19161-19172, 1998.
- McElroy, C.T., A spectroradiometer for the measurement of direct and scattered solar irradiance from on-board the NASA ER-2 high-altitude research aircraft, *Geophys. Res. Lett.*, *22*, 1361-1364, 1995.
- McElroy, M.B., R.J. Salawitch, and K. Minschwaner, The changing stratosphere, *Planet. Space Sci.*, *40*, 373-401, 1992.
- McPeters, R.D., et al., Earth Probe Total Ozone Mapping Spectrometer (TOMS) Data Products User's Guide, *NASA Tech. Pub. 1998-206895*, 64 pp., 1998.
- Montzka, S.A., J.H. Butler, R.C. Myers, T.M. Thompson, T.H. Swanson, A.D. Clarke, L.T. Lock, and J.W. Elkins, Decline in the tropospheric abundance of halogen from halocarbons: Implications for stratospheric ozone depletion, *Science*, *272*, 1318-1322, 1996.
- Osterman, G.B., B. Sen, G.C. Toon, R.J. Salawitch, J.J. Margitan, J.-F. Blavier, D.W. Fahey, and R.S. Gao, The partitioning of reactive nitrogen species in the summer Arctic stratosphere, *Geophys. Res. Lett.*, *26*, 1157-1160, 1999.
- Prather, M.J., Ozone in the upper stratosphere and mesosphere, *J. Geophys. Res.*, *86*, 5325-5338, 1981.
- Proffitt, M.H., K. Aikin, J.J. Margitan, M. Loewenstein, J.R. Podolske, A. Weaver, K.R. Chan, H. Fast, and J.W. Elkins, Ozone loss inside the northern polar vortex during the 1991-1992 winter, *Science*, *261*, 1150-1154, 1993.
- Robinson, G.N., D.R. Worsnop, J.T. Jayne, C.E. Kolb, and P. Davidovits, Heterogeneous uptake of ClONO₂ and N₂O₃ by sulfuric acid solutions, *J. Geophys. Res.*, *102*, 3583-3601, 1997.
- Rosenlof, K.H., Summer hemisphere differences in temperature and transport in the lower stratosphere, *J. Geophys. Res.*, *101*, 19129-19136, 1996.
- Saastad, O.W., T. Ellermann, and C.J. Nielsen, On the adsorption of NO and NO₂ on cold H₂O/H₂SO₄ surfaces, *Geophys. Res. Lett.*, *20*, 1191-1193, 1993.
- Salawitch, R.J., et al., The distribution of hydrogen, nitrogen, and chlorine radicals in the lower stratosphere: Implications for changes in O₃ due to emission of NO_x from supersonic aircraft, *Geophys. Res. Lett.*, *21*, 2547-2550, 1994a.
- Salawitch, R.J., et al., The diurnal variation of hydrogen, nitrogen, and chlorine radicals: Implications for heterogeneous production of HNO₂, *Geophys. Res. Lett.*, *21*, 2551-2554, 1994b.
- Schoeberl, M.R., S.D. Doiron, L.R. Lait, P.A. Newman, and A.J. Krueger, A simulation of the Cerro Hudson SO₂ cloud, *J. Geophys. Res.*, *98*, 2949-2955, 1993.
- Smith, K.W., R.M. Noyes, and P.G. Bowers, Gas evolution oscillators, 2, A reexamination of formic acid dehydration, *J. Phys. Chem.*, *87*, 1514-1519, 1983.
- Steele, H.M., and P. Hamill, Effects of temperature and humidity on the growth and optical properties of sulphuric acid-water droplets in the stratosphere, *J. Aerosol Sci.*, *12*, 517-528, 1981.
- Stimpfle, R.M., et al., The coupling of ClONO₂, ClO, and NO₂ in the lower stratosphere from in situ observations using the NASA ER-2 aircraft, *J. Geophys. Res.*, this issue.
- Tolbert, M.A., J. Pfaff, I. Jayaweera, and M.J. Prather, Uptake of formaldehyde by sulfuric acid solutions: Impact on stratospheric ozone, *J. Geophys. Res.*, *98*, 2957-2962, 1993.
- Toon, G.C., et al., Comparison of MkIV balloon and ER-2 aircraft measurements of atmospheric trace gases, *J. Geophys. Res.*, this issue.
- Turco, R.P., R.C. Whitten, and O.B. Toon, Stratospheric aerosols: Observation and theory, *Rev. Geophys.*, *20*, 233-279, 1982.
- Wallington, T.J., J.M. Andino, J.C. Ball, and S.M. Japar, Fourier transform infrared studies of the reaction of Cl atoms with PAN, PPN, CH₃OOH, HCOOH, CH₃COCH₃, and CH₃COC₂H₅ at 295±2 K, *J. Atmos. Chem.*, *10*, 301-313, 1990.
- Wamsley, P.R., et al., Distribution of halon-1211 in the upper troposphere and lower stratosphere and the 1994 total bromine budget, *J. Geophys. Res.*, *103*, 1513-1526, 1998.
- Wennberg, P.O., et al., Twilight observations suggest unknown sources of HO₂, *Geophys. Res. Lett.*, *26*, 1373-1376, 1999.
- Webster, C.R., R.D. May, C.A. Trimble, R.G. Chave, and J. Kendall, Aircraft (ER-2) laser infrared absorption spectrometer (ALIAS) for in situ stratospheric measurements of HCl, N₂O, CH₄, NO₂, and HNO₃, *Applied Optics* *33*, 454-472, 1994.
- Wilson, J.C., M.R. Stolzenburg, W.E. Clark, M. Loewenstein, G.V. Ferry, K.R. Chan, and K.K. Kelly, Stratospheric sulfate aerosol in and near the Northern Hemisphere polar vortex: The morphology of the sulfate layer, multimodal size distributions, and the effect of denitrification, *J. Geophys. Res.*, *97*, 7997-8013, 1992.
- Wilson, J.C., et al., In situ observations of aerosol and chlorine monoxide after the 1991 eruption of Mount Pinatubo: Effect of reactions on sulfate aerosol, *Science*, *261*, 1140-1143, 1993.
- Wine, P.H., R.J. Aсталos, and R.L. Maudlin III, Kinetic and mechanistic study of the OH + HCOOH reaction, *J. Phys. Chem.*, *89*, 2620-2624, 1985.
- Zhang, R., M.-T. Leu, and L.F. Keyser, Sulfuric acid monohydrate: Formation and heterogeneous chemistry in the stratosphere, *J. Geophys. Res.*, *100*, 18845-18854, 1995.
- Zhang, R., M.-T. Leu, and L.F. Keyser, Heterogeneous chemistry of HONO on liquid sulfuric acid: A new mechanism of chlorine activation on stratospheric sulfate aerosols, *J. Phys. Chem.*, *100*, 339-345, 1996.

K. Drdla, R.F. Pueschel, and A.W. Strawa, Atmospheric Physics Branch, NASA Ames Research Center, Moffett Field, CA 95006. (katja@aerosol.arc.nasa.gov; rpueschel@mail.arc.nasa.gov; astrawa@mail.arc.nasa.gov)
 R.C. Cohen, Department of Chemistry, University of California, Berkeley, CA 94720. (rccohen@cchem.berkeley.edu)
 T.F. Hanisco, Department of Chemistry, Harvard University, Cambridge, MA 02138. (tom@huarp.harvard.edu)

(Received December 4, 1998; revised June 10, 1998; accepted June 10, 1998.)